Intermittent depolymerization of actin filaments is caused by photo-induced dimerization of actin protomers

Thomas Niedermayer[a,1], Antoine Jégou[b,1], Lionel Chièze[b], Bérengère Guichard[b], Emmanuèle Helfer[b], Guillaume Romet-Lemonne[b,2], Marie-France Carlier[b], and Reinhard Lipowsky[a,2]

[a]Theory and Bio-Systems, Max Planck Institute of Colloids and Interfaces, 14424 Potsdam, Germany; and [b]Cytoskeleton Dynamics and Motility Group, Laboratoire d'Enzymologie et Biochimie Structurales, Centre National de la Recherche Scientifique, 1 Avenue de la Terrasse, 91198 Gif-sur-Yvette, France

Edited by Ronald D. Vale, University of California, San Francisco, CA, and approved May 1, 2012 (received for review December 28, 2011)

Actin, one of the most abundant proteins within eukaryotic cells, assembles into long filaments that form intricate cytoskeletal networks and are continuously remodelled via cycles of actin polymerization and depolymerization. These cycles are driven by ATP hydrolysis, a process that also acts to destabilize the filaments as they grow older. Recently, abrupt dynamical changes during the depolymerization of single filaments have been observed and seemed to imply that old filaments are more stable than young ones [Kueh HY, et al. (2008) *Proc Natl Acad Sci USA* 105:16531–16536]. Using improved experimental setups and quantitative theoretical analysis, we show that these abrupt changes represent actual pauses in depolymerization, unexpectedly caused by the photo-induced formation of actin dimers within the filaments. The stochastic dimerization process is triggered by random transitions of single, fluorescently labeled protomers. Each pause represents the delayed dissociation of a single actin dimer, and the statistics of these single molecule events can be determined by optical microscopy. Unlabeled actin filaments do not exhibit pauses in depolymerization, which implies that, in vivo, older filaments become destabilized by ATP hydrolysis, unless this aging effect is overcompensated by actin-binding proteins. The latter antagonism can now be systematically studied for single filaments using our combined experimental and theoretical method. Furthermore, the dimerization process discovered here provides a molecular switch, by which one can control the length of actin filaments via changes in illumination. This process could also be used to locally "freeze" the dynamics within networks of filaments.

filament aging | filament stability | single filament microscopy | microfluidics | stochastic processes

Actin is one of the most abundant and highly conserved proteins in eukaryotic cells. The globular protein assembles into long filaments, which form a variety of different networks within the cytoskeleton. The dynamic reorganization of these networks is crucial for many essential processes in cell motility, cell adhesion, and cell division (1–3). This remodelling, which covers a wide range of time scales from milliseconds to hours, is based on dissipative cycles of actin polymerization and depolymerization, two processes that are coupled to ATP hydrolysis and, in vivo, are regulated by a large number of actin-binding proteins.

Both bulk solution measurements (4, 5) as well as electron (6) and fluorescence microscopy (7–9) of single filaments provided evidence that, in the absence of actin-binding proteins, the stability and turnover of actin filaments is primarily determined by the actin-bound nucleotides. When ATP-actin is incorporated into a filament, the actin-bound ATP is hydrolyzed into ADP and inorganic phosphate (P_i). This process proceeds in two steps: First, ATP is quickly cleaved into ADP · P_i, which remains in the binding pocket of the actin protomer, and, second, P_i is released very slowly (5, 9) leaving only ADP in the pocket. Furthermore, because ADP-actin dissociates much faster from the filament end than ADP · P_i-actin (5), with a dissociation rate that is increased by more than 30 times (9), one concludes that, as a result of ATP hydrolysis, the filament becomes less stable as it grows older. The detailed structural changes of the filament associated with ATP hydrolysis are not known, but recent X-ray fiber diffraction (10) and cryo electron microscopy (EM) (11) of oriented actin filament gels indicate that, during the overall transition from globular (G) to filamentous (F) actin, the molecular structure is transformed from a G-actin conformation, in which the two major domains of the actin protein are rotated against each other, to a flatter untwisted F-actin conformation. It has also been proposed that F-actin can exhibit both an open and a closed nucleotide binding pocket (12), corresponding to a different, scissors-like displacement of the two major protein domains. The latter polymorphism, originally referred to as "angular disorder" (13) or "lateral slipping" (14), has been reported in many (12) but not in all (11) EM studies.

The view that the stability of actin filaments is controlled by ATP hydrolysis has been recently challenged by Kueh et al (15, 16), who observed abrupt changes during the depolymerization of single filaments and correlated these changes with the structural polymorphism or plasticity as observed by EM (12). Indeed, Kueh et al argued that these changes reflect a remodelling of the filament structure from a relatively disordered, unstable state of young filaments to the conventional, stable helix state (17, 18) as the filaments grew older. Such a remodelling would have far-reaching implications for many actin-related processes in vivo; see, e.g., refs. 19–21.

Results

Intermittent Depolymerization of Actin Filaments. The single filaments studied in ref. 15 were attached to the glass surface of the measurement chamber by many cross-linking molecules, which could stall the depolymerization process (22). To avoid such a multiple anchorage of the filaments to the glass surface, we developed improved experimental setups, for which the filaments were attached only at their pointed ends and aligned by microfluidic flows (9); see Fig. 1 and Movies S1–S4. Filaments were elongated for a few minutes in a G-actin solution. The solution was then quickly replaced by a buffer without G-actin that initiated filament depolymerization. Using fluorescence micro-

Author contributions: G.R.-L., M.-F.C., and R.L. designed research; T.N., A.J., L.C., B.G., E.H., G.R.-L., and R.L. performed research; T.N., A.J., G.R.-L., M.-F.C., and R.L. analyzed data; and T.N., A.J., G.R.-L., M.-F.C., and R.L. wrote the paper.

The authors declare no conflict of interest.

This article is a PNAS Direct Submission.

Freely available online through the PNAS open access option.

[1]T.N. and A.J. contributed equally to this work.

[2]To whom correspondence may be addressed. E-mail: lipowsky@mpikg.mpg.de or romet@lebs.cnrs-gif.fr.

This article contains supporting information online at www.pnas.org/lookup/suppl/doi:10.1073/pnas.1121381109/-/DCSupplemental.

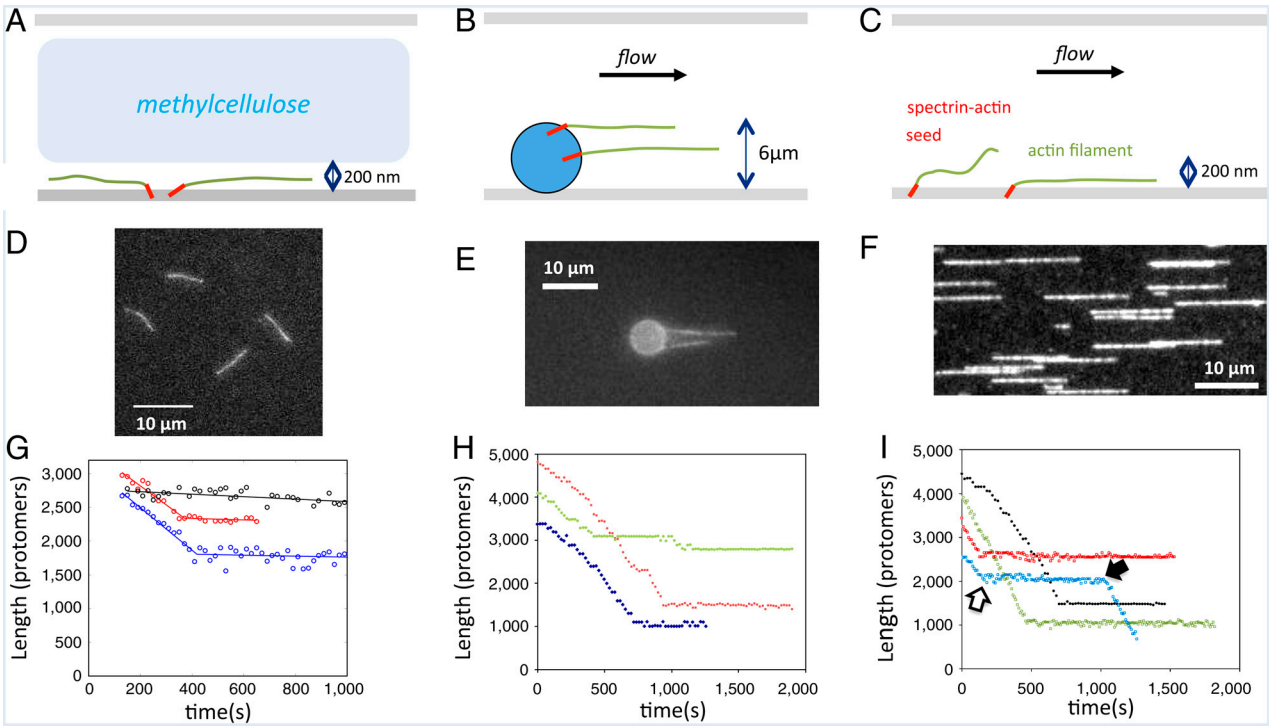

Fig. 1. Three different experimental setups for the observation of intermittent depolymerization. (*A*) Filaments are grown at spectrin-actin seeds anchored to the glass coverslip, and depolymerization is induced by a buffer with latrunculin that binds the dissociated G-actin. Methyl cellulose maintains the filaments within 200 nm from the coverslip, as confirmed by (*D*) total internal reflection fluorescence (TIRF) microscopy imaging, which allows (*G*) to monitor the length of the depolymerizing filaments; the black, red, and blue data points represent three different filaments grown from MgATP-actin. (*B*) and (*C*) Filaments are aligned by a continuous microfluidic flow, and depolymerization is induced by fast switching to a flow channel without actin. (*B*) Spectrin-actin seeds are anchored to 6-μm-diameter beads, (*E*) filaments are imaged a few microns above the glass coverslip using epifluorescence microscopy, and (*H*) their length is monitored during depolymerization; the red, green, and blue data points were obtained for three different filaments grown from MgATP-actin. (*C*) Spectrin-actin seeds are anchored to the glass coverlip, (*F*) filaments are imaged using TIRF or epifluorescence microscopy, and (*I*) their length is measured during depolymerization; black data points correspond to a filament grown from MgATP-actin whereas red, green, and blue data points were obtained for three filaments grown from MgADP-actin. One pause in depolymerization occurs between the white and black arrow in (*I*).

scopy, the length of individual filaments was monitored for tens of minutes; see Fig. 1 *G–I* and *Materials and Methods* section.

As shown in Fig. 1, filament depolymerization was typically interrupted after a few hundred seconds, and the filament length then attained a constant value for an extended, but finite period of time. These interruptions were also observed in filaments kept a few micrometers away from the surface and, thus, in the absence of any filament-surface interactions; see Fig. 1 *B*, *E*, and *H*. Filaments elongated from MgATP-actin, CaATP-actin, profilin-MgATP-actin, or MgADP-actin all displayed interruptions during depolymerization, whereas no such pauses were detected during polymerization. These results, together with the observations that depolymerizing MgADP · P_i-actin filaments, maintained in the ADP · P_i state by large bulk concentrations of P_i, and CrADP · P_i-actin filaments, which cannot release their P_i, also exhibit pauses, directly demonstrate that intermittent depolymerization is not coupled to ATP hydrolysis.

Furthermore, when pausing filaments were again exposed to G-actin and regrown by a few microns before switching back to depolymerization conditions, the second shrinking process was typically interrupted at precisely the same position at which the initial pause had occurred. More precisely, such a repeated interruption at the same filament position was observed for 86% of 131 regrown filaments, providing strong evidence that the interruptions are caused by local, nonpropagating changes in the filament structure; see Fig. 2*A* and Movie S5.

Local Protomer Transitions at Random Filament Sites. In general, one can envisage a variety of local interruption mechanisms: copolymerization of actin with another molecular species; tethering of a certain fraction of protomers to the surface of the cover slip; transient anchoring of the barbed end at the cover slip surface (8) (see Movie S4); or small concentrations of capping protein that occasionally bind to the barbed end. Even though these mechanisms are quite plausible, they can all be ruled out by a systematic data analysis, which focuses on the duration τ of the initial shrinking phase. As shown in Fig. 1, this time period represents a stochastic variable. It turns out that the statistical properties of this variable provide a surprisingly restrictive criterion for the interruption mechanism; see *SI Text* on *Theoretical Analysis*. Indeed, all four local mechanisms mentioned above would lead to an exponential distribution for the initial shrinking phase duration τ;see red lines in Fig. 2 *B* and *C*. The same distribution would also be obtained for a global structural transformation of the filament as proposed by Kueh et al (15, 16). Inspection of Fig. 2 *B* and *C* clearly shows, however, that such a distribution does not agree with the experimental data.

In contrast, a good description of the data is obtained if one considers another local process, in which actin protomers at random filament sites undergo transitions from an initial to a transformed state. The depolymerization process is now interrupted as soon as the shrinking filament end reaches such a transformed protomer. We developed a systematic theory for such a combined process; see *SI Text* on *Theoretical Analysis* as well as Figs. S1 and S2. The kinetics of this process depends on the depolymerization velocity v_{dep}, the rate ω of the random protomer transitions, and the polymerization velocity v_{pol}, which determines the age of the protomers within the filaments. The velocities v_{pol} and v_{dep} can be directly deduced from the observed kymographs as in Fig. 2*A* while the protomer transition rate ω can be determined from

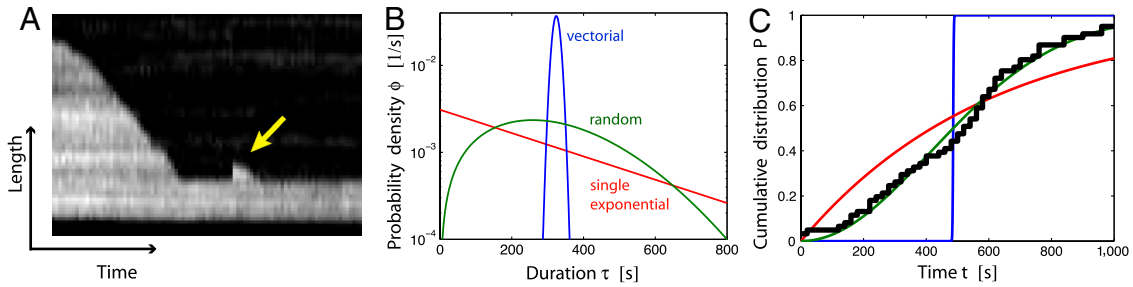

Fig. 2. Interruptions of depolymerization arise from local transitions at random filament sites. (*A*) After the interruption of initial depolymerization, we switched first to polymerization conditions for a short time period and then back to depolymerization conditions. The depolymerizing filament displayed a second interruption at precisely the same position, at which the first interruption had occured, see small "shark fin" indicated by the arrow. (*B*) Alternative probability densities for the duration τ of the initial shrinking phase (semilogarithmic plot). The red curve represents a single exponential distribution, the blue one corresponds to a putative vectorial process, and the green one to random protomer transitions. (*C*) Comparison of theoretical and experimental results for the cumulative distribution, i.e., the probability that the interruption occurs at any time prior to time t. The colored lines, which represent the same mechanisms as in (*B*), were obtained by least-square-fitting to the experimental data (black) using the transition rate ω as the only fit parameter. The green line for random transitions leads to the rate $\omega \simeq 10^{-6}$/s. The data were obtained from 61 filaments, polymerized from MgATP-actin using the microfluidics setup in Fig. 1*C*.

the cumulative distribution function of the random process. For the experimentally relevant range of parameters, this distribution function has the simple form

$$P(t) = 1 - e^{-\frac{1}{2}\alpha\omega t^2} \quad \text{with } \alpha \equiv v_{\text{dep}}(1 + v_{\text{dep}}/v_{\text{pol}}), \qquad [1]$$

which has a sigmoidal shape in agreement with the experimental data, see the green curve in Fig. 2*C*. This distribution implies the average duration $\langle\tau\rangle = (\pi/2\alpha\omega)^{1/2}$ of the fast initial phase. We also showed via control experiments that the transition rate ω was not affected by the flow rate in the microfluidics setup; see Fig. S3.

Transitions of Single, Fluorescently Labeled Protomers. To elucidate the molecular nature of the transformed protomer states, we varied the fraction X_{fl} of the fluorescently labeled actin protomers. The protomer transition rate ω was found to increase monotonically both with increasing fraction X_{fl} (Fig. 3*A*, *Inset*) and with the time-averaged illumination intensity (Fig. 3*B*, *Inset*). In addition, the microfluidics setup enabled us to study the depolymerization of unlabeled filament segments that were only briefly exposed to light; see Fig. 3 *C* and *D*. The latter experiments indicate that no transitions occur for unlabeled and unexposed F-actin. This conclusion was confirmed by control experiments on unexposed F-actin solutions (Fig. 4*A*), which also show that no dimers are formed in unexposed and labeled F-actin.

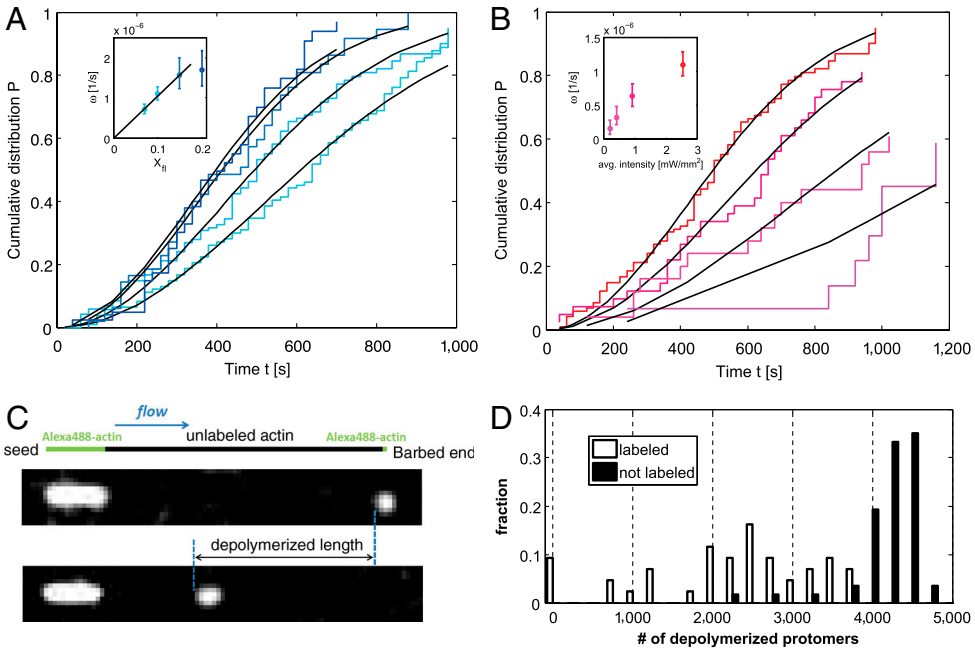

Fig. 3. Interruptions of depolymerization arise from photo-induced transitions of single, fluorescently labeled protomers: (*A*, *B*) Cumulative distribution functions P versus time t, as measured by epifluorescence microscopy with the experimental setup in Fig. 1*C*. (*A*) Variation of labeling fraction for constant time-averaged illumination intensity of 2.54 mW/mm^2: The four sets of data correspond to labeling fractions $X_{\text{fl}} = 0.07$, 0.1, 0.15, and 0.2 (bottom to top); the black lines are least-square fits to Eq. **1** with the transition rate ω as the only free parameter. (*Inset*) Rate ω as a function of X_{fl}. The error bars indicate confidence intervals of at least 50%; see *Materials and Methods* section. (*B*) Variation of illumination intensity for constant fraction $X_{\text{fl}} = 0.1$: The four sets of data correspond to time-averaged illumination intensities of 0.21, 0.42, 0.93, and 2.54 mW/mm^2 (bottom to top); the black lines are again least-square fits to Eq. **1**. (*Inset*) Rate ω as a function of time-averaged illumination intensity. (*C*) Depolymerization of unlabeled filament segments: A labeled segment, a long unlabeled segment, and a very short labeled segment (*Top*) were successively polymerized. The filament was then depolymerized for 15 min, before again polymerizing a short labeled segment (*Bottom*). (*D*) During the depolymerization phase of 15 min, the unlabeled segments lost about 4,000 to 4,500 protomers (black bars), as expected for a depolymerization velocity of $v_{\text{dep}} \simeq 5$/s indicating that unlabeled filaments depolymerize without interruptions. For comparison, the number of protomers lost by labeled filaments (white bars) is governed by a broad distribution indicating interruptions at different filament sites.

The data for small labeling fractions $X_{fl} = 0.07$, 0.1, and 0.15 are well described by the linear relation $\omega \approx X_{fl}\omega_{fl}$ for small X_{fl} with $\omega_{fl} \simeq 10^{-5}$/s for a time-averaged illumination intensity of 2.54 mW/mm^2; see Fig. 3*A*, *Inset*. This linear dependence on the labeling fraction, which was confirmed by control experiments on F-actin solutions (Fig. S4) implies that the local transitions typically involve only a single fluorescently labeled protomer and that these protomers are transformed with rate ω_{fl}. Indeed, a putative interaction between two such protomers would lead to a quadratic dependence of the protomer transition rate on the labeling fraction. Because of the low value of ω_{fl}, less than 1% of the fluorescently labeled protomers has been transformed after 10 min of illumination, even for the strongest illumination intensity used here.

Photo-Induced Formation and Delayed Dissociation of Actin Dimers. Finally, a series of additional experiments showed that these photo-induced transitions lead to the formation of actin dimers within the filament. First, solutions of fluorescently labeled F-actin were illuminated and subsequently analyzed via gel electrophoresis and immunodetection, which revealed the presence of stable actin dimers; see Fig. 4*A*, Fig. S4, and *SI Text* on *Western Blots*. The apparent molecular mass of these dimers was similar to the one of preformed lateral dimers that were obtained by covalent, pPDM-induced cross-links (23) between two protomers (24). For the fluorescently labeled F-actin, the dimer-to-monomer ratio increased linearly with the labeling fraction; see Fig. S4. Second, copolymerization of G-actin monomers with purified pPDM-cross-linked dimers induced additional pauses during depolymerization. As shown in Fig. 4*B*, the preformed dimers behave as a second species of transformed protomers that were present from the very beginning. The pauses induced by pPDM-cross-linked dimers had an average duration that was comparable to the one for photo-induced pauses, the latter being about 910 s for the data in Fig. 2*C*; see Fig. 5.

In principle, a photo-induced pause of depolymerization could be terminated via two alternative pathways, namely (*i*) by the dissociation of the photo-induced dimer from the filament or (*ii*) by the dissociation of the dimer into two protomers followed by the subsequent dissociation of these protomers from the filament. The latter two-step process can be ruled out for the preformed dimers, because these dimers are connected by covalent cross-links. For the photo-induced dimers, the Western blots in Fig. 4*A* strongly indicate that these dimers are covalently cross-linked as well. Furthermore, preformed and photo-induced dimers exhibit a similar pause statistics governed by a single exponential (see Fig. 5), which implies a single pathway. Thus, we conclude that the photo-induced dimers are covalently cross-linked and that the photo-induced pauses are terminated by the dissociation of these dimers from the filaments. From the data in Fig. 5, the dissociation rate ω_{pho} of the photo-induced dimers is found to be about 1.1×10^{-3}/s, which is much smaller than the dissociation rate of about 6/s for single ADP-actin protomers (9). This reduced dissociation rate reflects the additional molecular bonds between the dimer and the neighboring protomers at the barbed end and corresponds to an increase in the corresponding free energy barrier by about 8.6 k_BT compared to a terminal protomer as follows from transition state theory.

Discussion

In summary, we have shown that intermittent depolymerization of single actin filaments is neither coupled to actin-bound nucleotides nor does it reflect the structural polymorphism of F-actin as observed in EM. Thus, in contrast to the view expressed in refs. 15 and 16, our results do not provide any evidence that this polymorphism affects the stability of the filaments. Instead, we discovered that the interruptions or pauses of depolymerization arise from photo-induced transitions of fluorescently labeled protomers (Fig. 3), which trigger the formation of covalent actin dimers within the filaments; see Fig. 4. The linear dependence of the transition rate ω on the labeling fraction (Fig. 3*A*, *Inset*) implies that the dimerization reaction typically involves a single, fluorescently labeled protomer. The excited state of the fluorophore can provide energy for the production of reactive molecular species (25) that may then lead to the dimerization of two nearby actin protomers. The depolymerization process is interrupted as soon as an actin dimer becomes the terminal protomer at the filament end (see white arrow in Fig. 1*I*) and is continued when this protomer dissociates from the filament (see black arrow in Fig. 1*I*). Thus, each pause represents the delayed dissociation of a single dimer, which can be directly observed in the microscope, and the measured distribution of pause durations provides the statistics of these single molecule events; see Fig. 5. Because unlabeled filaments depolymerize without pauses (Fig. 3 *C* and *D*), our results support the view that filament stability and turnover is controlled by ATP hydrolysis and that actin filaments become less stable as they grow older in the absence of actin-binding proteins.

In the experiments described here, we primarily used the fluorophore Alexa 488 bound to surface lysines of the actin protein

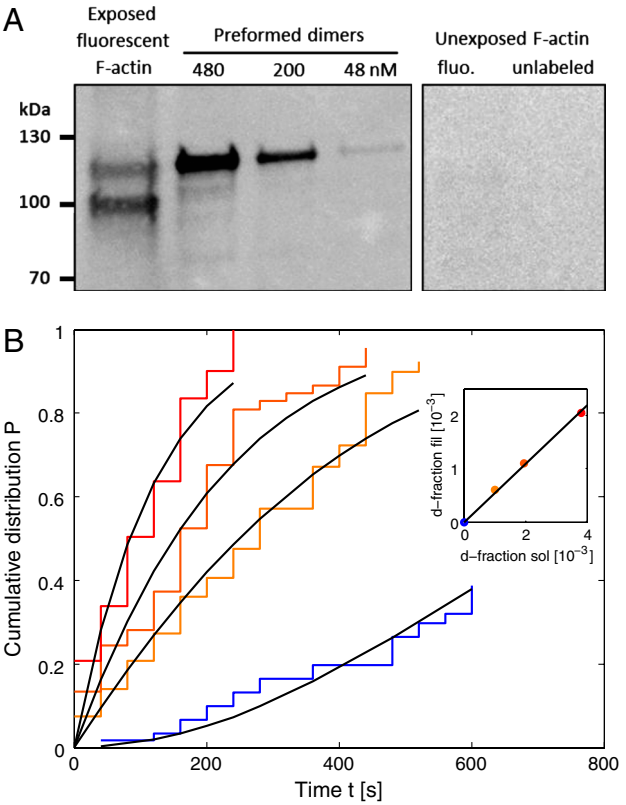

Fig. 4. Illumination of fluorescently labeled F-actin creates actin dimers as revealed by comparison with preformed, covalently cross-linked dimers. (*A*, *Left*) Western blots obtained with an actin antibody. The apparent molecular masses of the photo-induced dimers (left column) are compared with the corresponding masses of the preformed dimers (three columns on the right corresponding to three different bulk concentrations of preformed actin dimers). The apparent mass of the actin dimers exceeds their true mass of 86 kDa because the cross-links lead to a branched polypeptide chain. (*A*, *Right*) No dimers could be detected in labeled or unlabeled F-actin solutions that were not exposed to light. (*B*) Cumulative distributions for the occurrence of pauses during the depolymerization of filaments grown from G-actin with labeling fraction $X_{fl} = 0.1$ in the presence of 0 (blue data), 2, 4, and 8 nM (three sets of reddish data) preformed actin dimers. The black lines represent calculated distributions as described in *SI Text* on *Theoretical Analysis*. The *Inset* shows the linear relationship between the mole fractions of the preformed dimers (d-fractions) in the filaments and in solution.

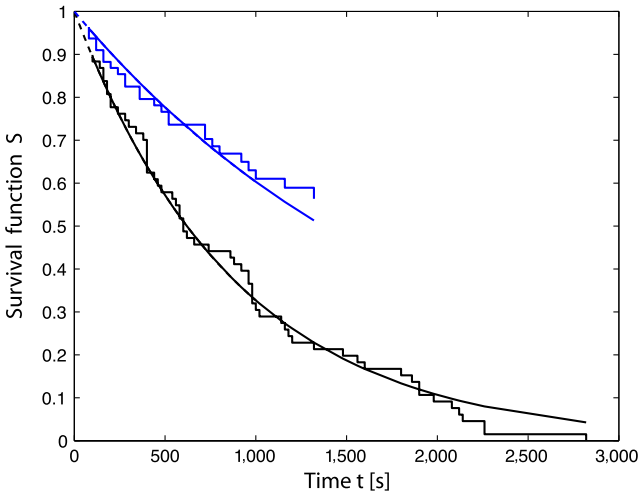

Fig. 5. Statistics for the durations of pauses caused by photo-induced and preformed dimers: Survival function S of terminal dimer versus time t for filaments elongated by copolymerization of actin monomers with 4 nM preformed actin dimers (blue data), and for filaments elongated from monomers alone (black data). The black and blue data correspond to the filaments analyzed in Fig. 2*C* and Fig. 4*B* (intermediate set of reddish data), respectively. The function $S = S(t)$ describes the probability that the terminal dimer remains attached to the barbed end for time periods that exceed t. Pause durations below about 80 s cannot be reliably detected because of the limited resolution of the optical microscope. The data are well fitted by a single exponential function $S(t) = \exp\{-\Omega t\}$ with $\Omega = \omega_{pho} = 1.1 \times 10^{-3}$/s for filaments with photo-induced dimers only (black line) and $\Omega = \hat{\omega}_{pre} = 5.1 \times 10^{-4}$/s for filaments with both preformed and photo-induced dimers (blue line). In the latter case, we conclude from Fig. 4*B* that at least three out of four pauses are caused by preformed dimers. Therefore, the dissociation rate ω_{pre} of preformed dimers is only slightly smaller than $\hat{\omega}_{pre}$ and the ratio $\omega_{pho}/\omega_{pre}$ for the dissociation rates of photo-induced and preformed dimers is smaller than 5. Transition state theory then implies that the free energy barriers for the dissociation of photo-induced and preformed dimers differ by less than 2 k_BT.

but we also observed intermittent depolymerization and photo-induced dimerization for filaments labeled with Alexa 594 or Atto 594 bound to actin's lysines and with Alexa 488 bound to Cys-374 of actin; see Fig. S5. Likewise, pauses in actin depolymerization have been observed for labeling with Alexa 647 on lysines (15, 16) and oregon green on Cys-374 (8). Photo-induced oligomerization of actin was also found in solutions of fluorescein-labeled and rhodamine-labeled actin (25). In the latter study, it was concluded from measurements of the viscosity that the filaments underwent photo-induced fragmentation, similar to microtubules (26). In contrast, the fluorophores studied here did not induce any appreciable fragmentation: Our study implies that the local fragmentation rate is much smaller than the rather low dimerization rate, and that photo-induced dimerization is the dominant structural modification of the filaments. Control experiments have shown that photo-induced dimerization can also take place in illuminated solutions of labeled G-actin (Fig. S4 and *SI Text* on *Western Blots*) but this process should be negligible in conventional microscopy experiments and certainly played no role in our microfluidics experiments because the filaments elongated from fresh G-actin that constantly entered the flow cell, without being previously illuminated.

The combined experimental and theoretical method described here provides a unique probe for the interactions between actin protomers and, thus, for the stability and turnover of single filaments. This probe is rather sensitive and can detect changes of less than 1 k_BT in dimer–protomer or protomer–protomer interactions; compare Fig. 5. Such changes may be induced by a variety of actin-binding molecules and proteins. Of particular interest are proteins such as tropomyosin, heavy meromyosin, or the Arp2/3 complex that bind to more than one actin protomer and may induce additional pauses in depolymerization. Another intriguing process, to which our method can be applied, is competitive binding of proteins to actin. Tropomyosin, for example, prevents cofilin (27) as well as Arp2/3 (28) from binding to actin whereas fimbrin prevents the binding of tropomyosin (29). The kinetics of these processes may be crucial for the coexistence of distinct actin networks within eukaryotic cells, a rather puzzling feature of the actin cytoskeleton (21, 30).

The fluorescently labeled actin proteins studied here act as molecular switches that can be used to interrupt the depolymerization of actin filaments and, thus, to control the length of the filaments (Fig. 1). Our results imply that the average interruption time $\langle\tau\rangle$ can be easily varied over at least one order of magnitude from a few hundred to several thousand seconds by changing the labeling fraction and/or the illumination intensity. When these molecular switches are incorporated into large networks of actin filaments and illuminated by focussed laser beams, one can 'freeze' the filament dynamics within localized regions of the networks. Using a procedure similar to fluorescence speckle microscopy (31), it may even be feasible to apply these molecular switches in vivo and, in this way, extend the method of "chromophore assisted laser inactivation" (32) from the protein to the filament level.

Materials and Methods

Proteins and Buffers. Actin was purified from rabbit muscle (33) and labeled with Alexa488 succinimidyl ester. The fraction of labeled actin (labeling fraction) was varied between 7 and 20%. Spectrin-actin seeds were purified from human erythrocytes. F-buffer contained 5 mM Tris pH 7.8, 0.2 mM ATP, 0.1 mM $CaCl_2$, 0.01% NaN_3, 100 mM KCl, 1 mM $MgCl_2$, 0.2 mM EGTA, and 1 mM DTT. Standard elongation and depolymerization of filaments was done in F-buffer, to which additionally 9 mM DTT and 1 mM diazabicyclooctane (DABCO) were added to limit photobleaching. In the experimental setup corresponding to Fig. 1*A*, the depolymerization buffer was additionally supplemented with 0.2 wt.% methyl cellulose M-0512 from Sigma and 3 μM latrunculin A. ATP-free buffer was used for experiments with ADP-actin.

Experimental Setups and Protocols. For the experiment shown in Fig. 1*A*, parafilm, a cleaned coverslip, and a microscopy slide were used to assemble the flow chamber that was first incubated with spectrin-actin seeds and then with 1–5% (wt/vol) bovine serum albumin (BSA) from Sigma. The polymerization solution containing 5 μM of actin was mixed in a tube and immediately flowed into the chamber. Depolymerization was initiated by rinsing with buffer and then flowing in the depolymerization buffer containing methyl cellulose and latrunculin A. By observing with TIRF microscopy, we checked that methyl cellulose maintains the filaments within 200 nm from the coverslip, ensuring that the error from the projection is small. Latrunculin A sequesters free actin monomers and ensures a G-actin concentration that is much smaller than the critical concentration (34). For the experimental setup shown in Fig. 1*C*, we constructed flow cells with poly dimethyl siloxane (PDMS) from Sylgard, mounted on standard glass coverslips that were previously cleaned in 1 M NaOH. Molds made of SU-8 photoresist were built at the clean room of the Ecole Superieure de Physique et de Chimie Industrielles (Paris), with the assistance of Hélène Berthet. The microchambers used were Y- or trident-shaped, having two or three entry channels, respectively. The microchannels were 42 μm high, and 200–800 μm wide. After adsorption of spectrin-actin seeds, the surface of the coverslip was passivated with BSA. Flow rates were controlled and monitored using a MAESFLO system (Fluigent). For each channel, the flow rate could be changed instantly throughout the experiment, between zero and a few tens of μL/min. For flow rates below 1 μL/min, the filaments fluctuated thermally away from the surface and were difficult to image. For flow rates above 5 μL/min, the filaments aligned with the flow, and the amplitude of thermal fluctuations was reduced. Observations were carried out between 1 and 3 mm downstream of the entry channel junction. This microfluidics setup is described in detail in ref. 9. It allows fluorescence microscopy of the filaments during the whole experiment and buffer exchange within less than 1 s. It was employed in the experiments shown in Figs. 2–5. All measurements reported here were performed at room temperature.

Image Acquisition and Analysis. Observations were carried out using an inverted Olympus IX71 microscope, with a 60x objective (and an additional

1.6x magnification in some cases), using TIRF or epifluorescence. Images were acquired by a Cascade II camera (Photometrics). For TIRF microscopy, a 25 mW laser from Cobolt, emitting at 473 nm, was used for the fluorescence excitation. For epifluorescence microscopy, a X-Cite 120Q light source from Lumen Dynamics was used. The optical microscopy was controlled using Metamorph. The time interval between images was 20 s, unless stated otherwise. Image stacks were analyzed using ImageJ. To obtain the length-vs.-time traces from the images as in Fig. 1*D*, we used a Java-based tracking program that was developed in the Vavylonis lab (35) and applies an open active contour model, to automatically measure the length of filaments. As most traces appear to be biphasic, we automatically determined a continuous and piecewise linear function with one kink that provided the best fit using the method of least squares. The kink of the fitting function determined the duration τ of the initial shrinking phase. For the images as in Fig. 1*F*, the contrast was enhanced using the KymoToolBox plugin (available from fabrice.cordelieres@curie.u-psud.fr). Again, filaments lengths were extracted from the images using the tracking program (35) and the initial shrinking phase duration τ was determined by inspection.

Because of the limited resolution of the optical microscope, we cannot reliably detect interruptions or pauses with a duration below about 80 s. However, as the pause durations are exponentially distributed with an average duration of about 1,000 s (Fig. 5), we conclude that we have missed at most 10% of the pauses. By monitoring the elongation of filaments, we have verified that filaments grew with a constant polymerization velocity v_{pol} that was compatible with the association rate constant $k_{\mathrm{on}} = 10\ \mu\mathrm{M\,s}^{-1}$ as determined in solution assays. Fragmentation events were rare, and pauses during elongation or annealing events were not observed. In our computations, each actin protomer was taken to contribute 2.7 nm to the filament length. A certain fraction of filaments did not depolymerize at all. Even for identical experimental conditions, this fraction varied between a few and 15% in an unreproducible manner. However, when we discarded these nondepolymerizing filaments, we obtained very reproducible results for the cumulative distribution functions.

Empirical Cumulative Distribution Functions. The cumulative distribution function $P = P(t)$ describes the probability that the interruption has occurred up to the time t after the initiation of depolymerization. If all filaments in the experiment can be observed until time t, the best estimate for $P(t)$ is simply given by the fraction of filaments that already exhibited an interruption before time t. However, for a small labeling fraction and/or a low illumination intensity, the interruption times τ are large and the microfluidic flow leads to a significant number of filaments that fragment or detach from the cover slip before exhibiting the interruption. In statistical analysis, such a fragmentation/detachment event is referred to as "right-censoring," because the event of interest, the interruption, cannot be observed after fragmentation/detachment. What one does know, however, is that the interruption has not occurred before the censoring event. For this type of right-censored datasets, the best estimate for $P(t)$ is the Kaplan–Meier estimator (36, 37), which we have used to compute the empirical cumulative distribution functions (ECDF) as given by the multistep functions in Figs. 3–5.

To specify the error bars for the transition rate ω as shown in Fig. 3, we proceeded as follows. The upper and lower confidence bounds for the ECDF were determined by Greenwood's formula (37), where a confidence level of 70% was chosen. Both confidence bounds were fitted to Eq. **1** of the main text and in each case, the 70% confidence interval for the parameter ω was determined. The lower bound of the error bar is chosen to be the lower parameter bound of the lower confidence bound of the ECDF. Analogously, the upper bound of the error bar is chosen to be the upper parameter bound of the upper confidence bound of the ECDF. Thus, the probability that the true value of ω lies within the error bar is at least $0.7 \times 0.7 \simeq 50\%$.

Further information on *Variation of Illumination* and *Copolymerization of Actin Monomers and Preformed Actin Dimers* can be found in the *SI Text*.

ACKNOWLEDGMENTS. We thank Jan Kierfeld for stimulating discussions as well as Hermann Gaub, Paul Janmey, Jean-Francois Joanny, Edward Korn, and Helmuth Möhwald for critical comments on an earlier version of this manuscript. G.R.L. acknowledges support from the Human Frontier Science Program (Grant RGY0067/2008). M.F.C. acknowledges support from Agence Nationale de la Recherche–Physique et Chimie du Vivant program 2006, the Ligue Nationale contre le Cancer (équipe labellisée), the European Union Seventh Framework Program (MitoSys, Grant 241548), and a European Research Council advanced grant (ERC 2009-249982-Forcefulactin).

1. Bray D (2001) *Cell Movements* (Garland, New York).
2. Pollard TD, Earnshaw W, Lippincott-Schwartz J (2007) *Cell Biology* (Saunders, Philadelphia), 2nd Ed.
3. Bugyi B, Carlier MF (2010) Control of actin filament treadmilling in cell motility. *Ann Rev Biophys* 39:449–470.
4. Carlier MF, Pantaloni D, Korn ED (1984) Evidence for an ATP cap at the ends of actin filaments and its regulation of the F-actin steady state. *J Biol Chem* 259:9983–9986.
5. Carlier MF, Pantaloni D (1988) Binding of phosphate to F-ADP-actin and role of F-ADP-P_i-actin in ATP-actin polymerization. *J Biol Chem* 263:817–825.
6. Pollard TD (1986) Rate constants for the reactions of ATP- and ADP-actin with the ends of actin filaments. *J Cell Biol* 103:2747–2754.
7. Fujiwara I, Takahashi S, Tadakuma H, Funatsu T, Ishiwata S (2002) Microscopic analysis of polymerization dynamics with individual actin filaments. *Nat Cell Biol* 4:666–673.
8. Kuhn JR, Pollard TD (2005) Real-time measurements of actin filament polymerization by total internal reflection fluorescence microscopy. *Biophys J* 88:1387–1402.
9. Jégou A, et al. (2011) Individual actin filaments in a microfluidic flow reveal the mechanism of ATP hydrolysis and give insight into the properties of profilin. *PLoS Biol* 9:e1001161.
10. Oda T, Iwasa M, Aihara T, Maeda Y, Narita A (2009) The nature of the globular-to fibrous-actin transition. *Nature* 457:441–445.
11. Fujii T, Iwane AH, Yanagida T, Namba K (2010) Direct visualization of secondary structures of F-actin by electron cryomicroscopy. *Nature* 467:724–728.
12. Galkin VE, Orlova A, Schröder GF, Egelman EH (2010) Structural polymorphism in F-actin. *Nat Struct Mol Biol* 17:1318–1323.
13. Egelman EH, Francis N, DeRosier DJ (1982) F-actin is a helix with a random variable twist. *Nature* 298:131–135.
14. Bremer A, et al. (1991) The structural basis for the intrinsic disorder of the actin filament: The "lateral slipping" model. *J Cell Biol* 115:689–703.
15. Kueh HY, Brieher WM, Mitchison TJ (2008) Dynamic stabilization of actin filaments. *Proc Natl Acad Sci USA* 105:16531–16536.
16. Kueh HY, Mitchison TJ (2009) Structural plasticity in actin and tubulin polymer dynamics. *Science* 325:960–963.
17. Oda T, Maeda Y (2010) Multiple conformations of F-actin. *Structure* 18:761–767.
18. Dominguez R, Holmes KC (2011) Actin structure and function. *Annu Rev Biophys* 40:169–186.
19. Mizuno H, et al. (2011) Rotational movement of the formin mDia1 along the double helical strand of an actin filament. *Science* 331:80–83.
20. Popp D, Robinson RC (2011) Many ways to build an actin filament. *Mol Microbiol* 80:300–308.
21. Michelot A, Drubin DG (2011) Building distinct actin filament networks in a common cytoplasm. *Curr Biol* 21:R560–R569.
22. Schmoller KM, Semmrich C, Bausch AR (2011) Slow down of actin depolymerization by cross-linking molecules. *J Struct Biol* 173:350–357.
23. Knight P, Offer G (1978) p-NN′-phenylenebismaleimide, a specific cross-linking agent for F-actin. *Biochem J* 175:1023–1032.
24. Elzinga M, Phelan J (1984) F-actin is intermolecularly crosslinked by NN′-p-phenylenedimaleimide through lysine-191 and cysteine-374. *Proc Natl Acad Sci USA* 81:6599–6602.
25. Simon JR, et al. (1988) Analysis of rhodamine and fluorescein-labeled F-actin diffusion in vitro by fluorescence photobleaching recovery. *Biophys J* 54:801–815.
26. Vigers GPA, Coue M, McIntosh JR (1988) Fluorescent microtubules break up under illumniation. *J Cell Biol* 107:1011–1024.
27. DesMarals V, Ichetovkin I, Condeells J, Hitchcock-DeGregori SE (2002) Spatial regulation of actin dynamics: A tropomyosin-free, actin-rich compartment at the leading edge. *J Cell Sci* 115:4649–4660.
28. Bugyi B, Didry D, Carlier MF (2010) How tropomyosin regulates lamellipodial actin-based motility: A combined biochemical and reconstituted motility approach. *EMBO Journal* 29:14–26.
29. Skau CT, Kovar DR (2010) Fimbrin and tropomyosin competition regulates endocytosis and cytokinesis kinetics in fission yeast. *Curr Biol* 20:1415–1422.
30. Chhabra ES, Higgs HN (2007) The many faces of actin: Matching assembly factors with cellular structures. *Nat Cell Biol* 9:1110–1121.
31. Danuser G, Waterman-Storer CM (2006) Quantitative fluorescent speckle microscopy of cytoskeleton dynamics. *Annu Rev Biophys Biomol Struct* 35:361–387.
32. Jacobson K, Rajfur Z, Vitriol E, Hahn K (2008) Chromophore-assisted laser inactivation in cell biology. *Trends Cell Biol* 18:443–450.
33. Spudich JA, Watt S (1971) The regulation of rabbit skeletal muscle contraction I: Biochemical studies of interaction of tropomyosin-troponin complex with actin and the proteolytic fragments of myosin. *J Biol Chem* 246:4866–4871.
34. Coué M, Brenner S, Spector I, Korn E (1987) Inhibition of actin polymerization by latrunculin A. *FEBS Letters* 213:316–318.
35. Li H, et al. (2009) Automated actin filament segmentation, tracking, and tip elongation measurements based on open active contour models. *2009 IEEE International Symposium on Biomedical Imaging: From Nano to Macro*, Vols. 1 and 2 (Institute of Electrical and Electronics Engineers, Boston), pp 1302–1305.
36. Kaplan EL, Meier P (1958) Nonparametric estimation from incomplete observation. *J Am Stat Assoc* 53:457–481.
37. Kalbfleisch J, Prentice R (2002) *The Statistical Analysis of Failure Time Data* (Wiley & Sons, Hobokem, New Jersey), 2nd Ed.